Available online at www.sciencedirect.com
ScienceDirect
Mathematics and Computers in Simulation 224 (2024) 50–62
MATHEMATICS AND COMPUTERS IN SIMULATION
www.elsevier.com/locate/matcom

Original articles

Photovoltaic module series resistance identification at its maximum power production

Kari Lappalainen[a,*], Michel Piliougine[b], Seppo Valkealahti[a], Giovanni Spagnuolo[b]

[a] *Tampere University, Electrical Engineering Unit, 33720 Tampere, Finland*
[b] *University of Salerno, DIEM Department, 84084 Salerno, Italy*

Received 13 October 2022; received in revised form 12 May 2023; accepted 24 May 2023
Available online 1 June 2023

Abstract

Analysis of measured current–voltage curves offers a cost-effective option for online condition monitoring of photovoltaic (PV) modules. The current–voltage curves of PV modules can be modeled accurately using the well-known electrical single-diode model. In practical applications, condition monitoring should be based on measurements performed near the maximum power point (MPP) by affecting PV power production negligibly. The series resistance is the most important single-diode model parameter in assessing the condition of PV modules; this paper proposes a novel method for its determination by using measurements acquired near the MPP only. The proposed method can be used with any series resistance identification procedure based on current–voltage curve measurements. The proposed method is experimentally validated using current–voltage curves of two PV modules measured in Malaga, Spain. This study allows to assess that the series resistance can be accurately determined from measurements performed near the MPP. Especially the results obtained with an ISOFOTON ISF-145 PV module are very promising: the scaled series resistances obtained from measurements done without lowering the PV power more than 2% of the maximum power differ on the average by no more than 2% of the series resistances obtained from the whole current–voltage curves.

Keywords: Series resistance; Parametric identification; Condition monitoring; Photovoltaic module; Single-diode model; Curve fitting

1. Introduction

Condition monitoring of photovoltaic (PV) systems is vital to notice degradation, malfunctions, and contamination of PV modules and thus to maximize power production of the systems. The main drawback of currently used condition monitoring systems of PV modules and generators is that they are complex, expensive, and labor-intensive. For these reasons, uninterrupted condition monitoring of PV power plants is rarely applied in practice. Condition monitoring, for example by thermal cameras on board drones, is typically carried out at regular intervals. Utilization of measured current–voltage (I–V) curves provides a cost-effective solution for online condition monitoring of PV modules avoiding use of costly radiometric sensors [9] and thermal cameras [11] used in conventional monitoring methods. The I–V curves of PV modules can be modeled accurately under different irradiance and temperature

* Corresponding author.
E-mail addresses: kari.lappalainen@tuni.fi (K. Lappalainen), mpiliouginerocha@unisa.it (M. Piliougine), seppo.valkealahti@tuni.fi (S. Valkealahti), gspagnuolo@unisa.it (G. Spagnuolo).

https://doi.org/10.1016/j.matcom.2023.05.021
0378-4754/

Table 1
Comparison between existing series resistance identification methods.

References	*I–V* curve input	Required additional measurements
[10]	SC, OC, MPP	*T*
[5]	SC, OC, MPP	*G*, *T*
[13,16,17]	Entire or partial *I–V* curve	–
[3,18,27]	Entire or partial *I–V* curve	*T*
[1,2,30]	Entire or partial *I–V* curve	*G*, *T*

conditions using the well-known electrical single-diode model (SDM). The SDM contains aging and condition dependent parameters enabling condition monitoring based on parameter identification. The most important SDM parameter in assessing the condition of PV modules is series resistance. Increase of the series resistance reveals aging and faults of the modules [15].

Parameter values for the electrical models are typically identified in standard test conditions (STC), in which irradiance G (1000 W/m^2) and temperature T (25 °C) are known. The parameter values are then converted to other conditions based on their G and T behavior [4,29]. Thus, G and T measurements are required to identify parameter values under field conditions. Indeed, almost all procedures presented for parameter identification require operating condition measurements: measured temperature is required for the approaches presented in [3,10,18,27]; and temperature and irradiance measurements are required for the approaches proposed in [1,2,5,30]. The need of G and T measurements naturally restricts the use of identification procedures for on-site condition monitoring. Only a few procedures have been proposed to identify parameters from *I–V* curves without additional measurements [13,16,17]. Some methods focus on identification of only the series resistance instead of identifying multiple parameters. An overview of such methods is provided in [25]. An experimental validation of various explicit methods used to identify the SDM parameters was presented in [22] with the main emphasis on identification of the series resistance in presence of artificial degradation. Among the methods considered in [22], the one presented in [20] showed good capability to estimate the series resistance.

Some parameter identification methods require measurements of the three key points of *I–V* curves, i.e., open-circuit (OC), maximum power point (MPP), and short-circuit (SC), while some methods do not require OC and SC measurements. Required inputs of existing parameter identification methods are compiled in Table 1. All the listed methods include series resistance among the identified parameters. Measurement of the OC voltage and SC current or of the entire *I–V* curves interrupts electrical energy production and causes production losses. Thus, for practical applications, condition monitoring should be based on measurements performed near the MPP with minimal disruption of PV power production. That kind of an online method capable of reliably identifying aging and faults of the modules of a PV generator from simple electrical measurements with minimal interruption of PV power production could totally revolutionize condition monitoring of PV power plants and substantially reduce their operation and maintenance costs. Identification of series resistance from measurements performed near the MPP has been discussed earlier in only a few articles. The parameter identification procedures proposed in [16,17] were also validated with partial *I–V* curves containing only values measured near the MPP. In [12], selection of the vicinity of the MPP for parameter identification was studied using the identification method proposed in [13]. The results shown in [12,17] indicate that the series resistance can be identified accurately from measurements done in the vicinity of the MPP. A method to determine the faults based on computation of diagnostic indicators from *I–V* curves was proposed in [26] and, among others, equivalent series resistance was calculated from *I–V* curve slope near the MPP. However, further research is needed related to identification of the series resistance from measurements performed near the MPP in order to reach practical applications.

In this paper, a novel method for the determination of the series resistance from measurements performed near the MPP is proposed. The proposed method, which is experimentally validated using *I–V* curves of two PV modules measured in Malaga, Spain, is used jointly with the SDM parameter identification procedure presented in [17]. Nonetheless, it can be used with any series resistance identification procedure based on *I–V* curve measurements. The rest of this paper is organized as follows. The SDM parameter identification procedure used in this study is introduced in Section 2.1. Section 2.2 introduces the proposed series resistance determination method and Section 2.3 describes the used measurement data. The proposed determination method is experimentally validated in Section 3. Factors affecting the performance of the proposed method are discussed in Section 4. The conclusions of the study are provided in Section 5.

2. Methods and data

2.1. Identification procedure

PV modules were modeled with the SDM from which the basic implicit equation can be derived for the current and voltage of the module as follows

$$I = I_{\mathrm{ph}} - I_{\mathrm{s}}\left(e^{\frac{V+R_{\mathrm{s}}I}{\eta V_{\mathrm{t}}}} - 1\right) - \frac{V + R_{\mathrm{s}}I}{R_{\mathrm{sh}}}, \tag{1}$$

where I_{ph} is the light-generated current, I_{s} the dark saturation current, R_{s} the series resistance, η the ideality factor, V_{t} the thermal voltage, and R_{sh} the shunt resistance of the PV module [19]. The thermal voltage can be written as $V_{\mathrm{t}} = N_{\mathrm{s}}kT/q$, where N_{s} is the number of series-connected cells in the PV module, k the Boltzmann constant, T the PV cell temperature, and q the elementary charge.

In order to identify parameters G, T, R_{s}, and R_{sh} from measured I–V curves using Eq. (1), the values of I_{ph}, I_{s}, and η must be known. The light-generated current I_{ph} was calculated as

$$I_{\mathrm{ph}} = \frac{G}{G_{\mathrm{STC}}}\left(I_{\mathrm{SC,STC}}\left(\frac{R_{\mathrm{sh}} + R_{\mathrm{s}}}{R_{\mathrm{sh}}}\right) + \alpha_I\,(T - T_{\mathrm{STC}})\right), \tag{2}$$

where α_I is the thermal coefficient of I_{SC} [17]. The ideality factor η, which was kept at its STC value [7], was calculated as

$$\eta = \frac{\alpha_V - \frac{V_{\mathrm{OC,STC}}}{T_{\mathrm{STC}}}}{V_{\mathrm{t,STC}}\left(\frac{\alpha_I}{I_{\mathrm{ph,STC}}} - \frac{3}{T_{\mathrm{STC}}} - \frac{E_{\mathrm{g,STC}}}{kT_{\mathrm{STC}}{}^2}\right)}, \tag{3}$$

where α_V is the thermal coefficient of V_{OC} and $E_{\mathrm{g,STC}}$ is the material energy bang gap at STC [8]. The saturation current I_{s} was calculated as in [28]

$$I_{\mathrm{s}} = C_{\mathrm{STC}}T^{\frac{3}{\eta}}e^{\frac{-E_{\mathrm{g}}(T)}{\eta kT}}, \tag{4}$$

where the energy bang gap $E_{\mathrm{g}}(T)$ is calculated according to what is discussed in [7]

$$E_{\mathrm{g}}(T) = E_{\mathrm{g,STC}}\left(1 + \alpha_{E_{\mathrm{g}}}\,(T - T_{\mathrm{STC}})\right), \tag{5}$$

where $\alpha_{E_{\mathrm{g}}}$ is the thermal coefficient of E_{g}. A coefficient C_{STC} is calculated at STC by the approach presented in [17]

$$C_{\mathrm{STC}} = \frac{I_{\mathrm{ph,STC}}e^{\gamma_{\mathrm{STC}}}}{T_{\mathrm{STC}}{}^{\frac{3}{\eta}}}, \tag{6}$$

where

$$\gamma_{\mathrm{STC}} = -\frac{V_{\mathrm{OC,STC}}}{\eta V_{\mathrm{t,STC}}} + \frac{E_{\mathrm{g,STC}}}{\eta kT_{\mathrm{STC}}}. \tag{7}$$

The identification procedure is described in detail and its ability to identify the actual value of the series resistance is verified experimentally in [17]. Thus, the identified series resistance values can be considered as accurate approximations of the actual series resistance, which creates a valid basis for the experimental validation of the proposed series resistance determination method in Section 3.

The fitting procedure needs initial guess values for the unknown parameters $\{G, T, R_{\mathrm{s}}, R_{\mathrm{sh}}\}$. For the first curve of each dataset, STC values of the identified parameters are used as the initial guesses. The STC values of R_{s} and R_{sh} were calculated by the procedure presented in [19]. For that, η was calculated by Eq. (3), assuming that $I_{\mathrm{ph,STC}} = I_{\mathrm{SC,STC}}$, and $I_{\mathrm{s,STC}}$ was calculated by Eq. (4) using the STC values of T, η, and E_{g}. For all other I–V curves, the identified parameter set of the previous curve was used as the guess values. This requires that time interval between two consecutive curve measurements is not too long.

2.2. Proposed series resistance determination method

It was observed in [17] that identified series resistance typically increases when the portion of the I–V curve used for identification in the vicinity of the MPP decreases, i.e., the smaller is the portion of the curve around the

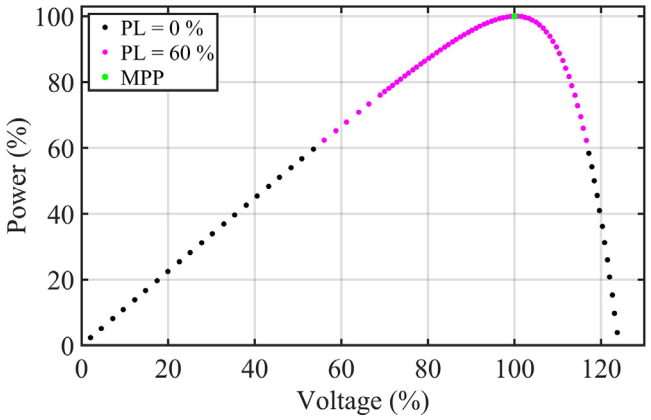

Fig. 1. Example of a measured *P–V* curve of the I-53 module with two power limits. The power and voltage are with respect to the MPP values.

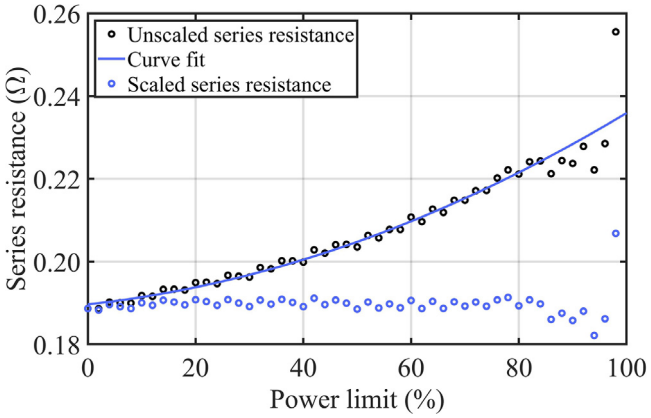

Fig. 2. Unscaled and scaled series resistances identified from a measured *I–V* curve of the ISF-145 module as a function of the power limit and curve fit to the unscaled values.

MPP used for the identification, the larger is the identified series resistance value. The method proposed in this paper for determining series resistance is based on the idea that this increase can be mathematically modeled, and the mathematical model could then be used to scale the series resistance values identified from the measurements made near the MPP to correspond to the value of the whole curve.

The share of the *I–V* curve used for the identification can be described by the concept of power limit (PL). Only the part of the curve with power higher than the PL is utilized for the identification. The PL is expressed with respect to the MPP power of the curve. The concept of power limit is illustrated in Fig. 1 where a measured *P–V* curve is presented with two PL values.

The series resistance identified from a measured *I–V* curve of the ISF-145 module is shown as a function of the PL in Fig. 2. The PL was varied from 0% (whole curve) to 98% (only the part that is within 2% from the MPP power). The second-degree polynomial curve fit to the identified series resistance values as a function of the power limit in Fig. 2 follows the equation

$$R_s = c_1 \mathrm{PL}^2 + c_2 \mathrm{PL} + c_3, \tag{8}$$

where c_1, c_2, and c_3 are fitting constants. As can be seen from Fig. 2, the fitted curve follows the identified series resistance values very well, especially at PL values up to 84%. As expected, the identified series resistance varies more at high PL values because only a small portion of the curve is used for the identification. To mitigate the effects of such variation, Eq. (8) was fitted to the averages of series resistances as a function of PL, identified from 10 *I–V* curves measured over a short period of time under nearly constant operating conditions.

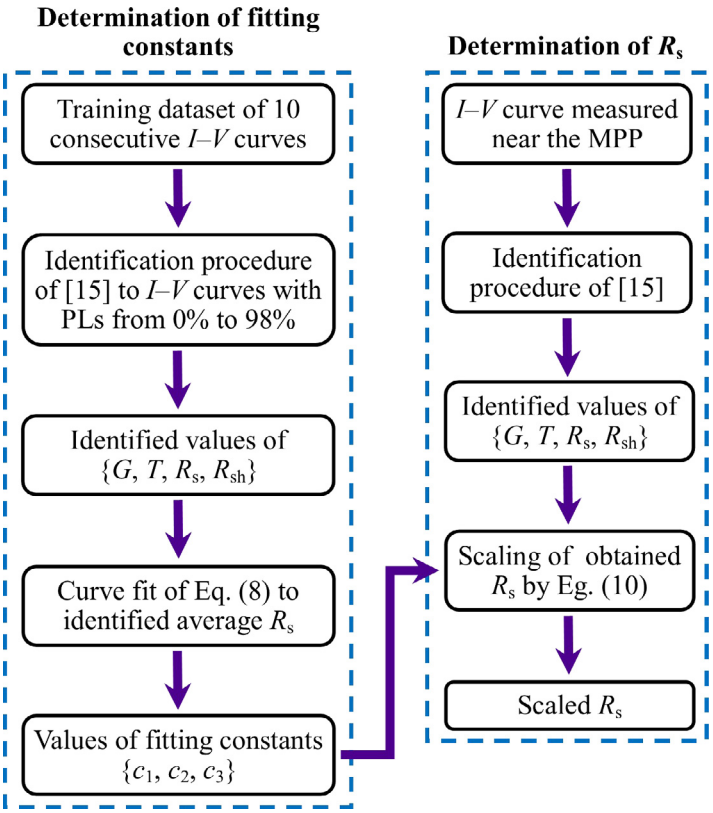

Fig. 3. Flowchart of the proposed series resistance determination method.

The curve fit of Eq. (8) can be used to scale the series resistance values identified in the vicinity of the MPP to correspond the values obtained using the whole curve. The following proportionality can be formed between the series resistance values identified from partial curves ($R_{s,unscaled}$) and the values corresponding to the use of the whole curve ($R_{s,scaled}$)

$$\frac{R_{s,unscaled}}{R_{s,scaled}} = \frac{c_1 PL^2 + c_2 PL + c_3}{c_3}, \tag{9}$$

from which the scaled series resistance is solved as

$$R_{s,scaled} = \frac{R_{s,unscaled} c_3}{c_1 PL^2 + c_2 PL + c_3}. \tag{10}$$

The proposed series resistance determination method is illustrated in Fig. 3. First, the identification procedure described in [17] is used to identify series resistance from 10 *I–V* curves, which serve as a training dataset, varying PL from 0% to 98%. Then, Eq. (8) is fitted to the obtained average series resistance of the 10 curves as a function of the PL to obtain values for the constants c_1, c_2, and c_3. Finally, series resistance values identified from *I–V* curves measured near the MPP are scaled using Eq. (10) and the obtained values of the fitting constants to correspond the values identified using the whole curve.

The proposed method for determining the series resistance is further illustrated in Fig. 2. At PL values up to 84%, the scaled series resistance is close to the one obtained using the whole curve and begins to deviate only at higher PL values. However, only the value corresponding to PL of 98% clearly differs from the trend. Even in this case, the scaled series resistance (0.207 Ω) is much closer to the value obtained with the whole curve (0.189 Ω) than the unscaled one (0.256 Ω).

Table 2
Electrical parameter values of the studied PV modules.

Parameter	ISOFOTON I-53	ISOFOTON ISF-145
$I_{SC,STC}$ (A)	2.56	8.55
$V_{OC,STC}$ (V)	20.5	22.4
$I_{MPP,STC}$ (A)	2.26	8.00
$V_{MPP,STC}$ (V)	16.5	18.1
α_I (A/K)	0.00102	0.00359
α_V (V/K)	−0.061	−0.072
N_s	36	36

Table 3
SDM parameter values of the studied PV modules in STC.

Parameter	ISOFOTON I-53	ISOFOTON ISF-145
η_{STC} (–)	0.88541	1.0041
$I_{ph,STC}$ (A)	2.56	8.55
$I_{s,STC}$ (A)	3.4425e−11	2.8646e−10
$R_{s,STC}$ (Ω)	0.60181	0.18235
$R_{sh,STC}$ (Ω)	90.167	131.43

2.3. Experimental dataset

The proposed series resistance determination method is validated using *I–V* curve measurements of two PV modules measured at the University of Malaga, Spain. The used data consist of 90 *I–V* curves of an ISOFOTON I-53 module measured on 29 July 2017 and 150 curves of an ISOFOTON ISF-145 module measured on 14 July 2014. Time intervals between consecutive measurements were from 6 to 7 s and from 9 to 10 s, for the I-53 and ISF-145 modules, respectively. Irradiances incident on the modules were measured by Kipp & Zonen CMP21 pyranometers and PV module temperatures were measured by Pt100 temperature sensors. The measurement system is described in detail in [21].

The electrical parameter values of the studied PV modules are listed in Table 2. For the ISF-145 module, datasheet values provided by the manufacturer were used. However, the values provided by the manufacturer for the I-53 module, which has been working for 21 years (by 2017), are no longer close to the actual ones. Thus, the values determined in [23] were used instead of the datasheet values. The studied modules are made of monocrystalline silicon PV cells. The calculated SDM parameter values in STC for the studied PV modules are presented in Table 3.

Both PV module datasets contain a period of 10 consecutive *I–V* curves measured under steady-state conditions, which are used for fitting Eq. (8) to obtain values for the constants c_1, c_2, and c_3. The rest of the measurement periods are used to test the performance of the proposed method. The fitted constant values of Eq. (8) obtained for the 10 curve periods are then used to scale the series resistances identified from the partial *I–V* curves measured during the rest of the measurement periods to correspond the values of the whole curve.

Measured operating irradiances and back-sheet temperatures during the 10 curve periods are presented in Figs. 4 and 5, respectively. The irradiances received by the I-53 and ISF-145 modules were nearly constant at 990 and 845 W/m^2, respectively, while the temperatures increased gradually. Figs. 4 and 5 show also irradiance and temperature values identified by the fitting procedure using the whole *I–V* curves. For both modules, the identified irradiance is a bit higher than the measured one. The identified cell temperature of the I-53 module is a bit lower than the measured back-sheet temperature while the identified cell temperature of the ISF-145 module is higher than the measured back-sheet temperature. Behavior of the identified irradiance and temperature values is in accord with the results of [17].

The performance of the proposed method is tested using 80 measured *I–V* curves of the I-53 module and 140 curves of the ISF-145 module. Figs. 6 and 7 show the measured and identified operating irradiances and temperatures during these periods for the I-53 and ISF-145 modules, respectively. The irradiance received by the I-53 module was nearly constant around the same values as in Fig. 4. The measured temperature increased from 17 to 44 °C during the period. For the ISF-145 module, both the measured irradiance and the measured temperature increased

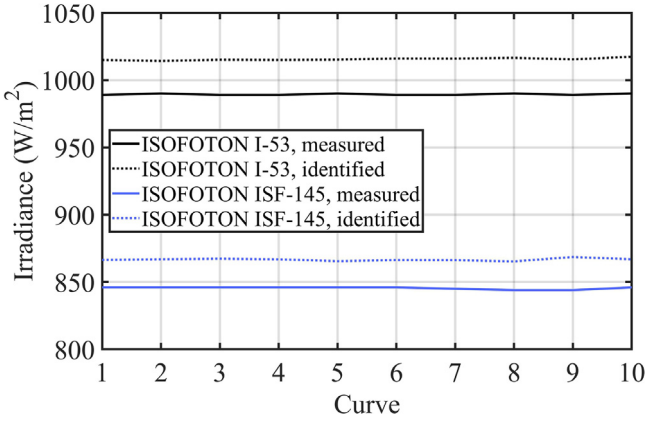

Fig. 4. Measured and identified irradiances of the I-53 and ISF-145 modules during the measurement periods of 10 *I–V* curves.

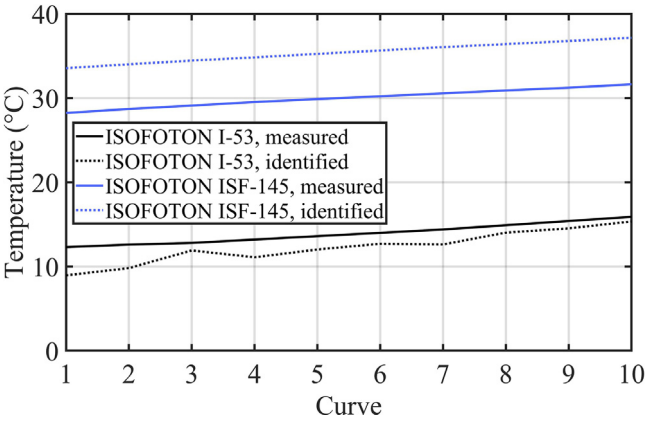

Fig. 5. Measured back-sheet temperatures and identified cell temperatures of the I-53 and ISF-145 modules during the measurement periods of 10 *I–V* curves.

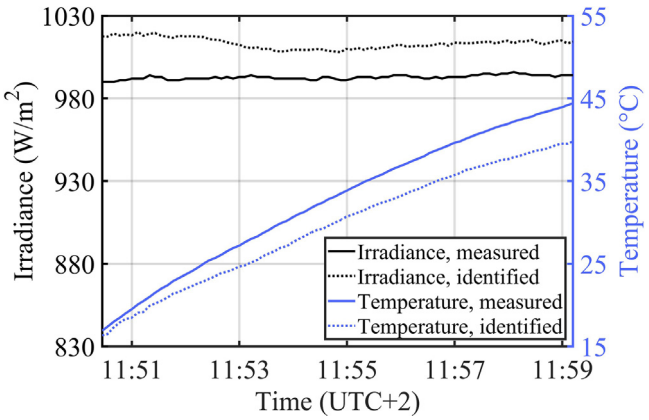

Fig. 6. Measured and identified irradiance and temperature for the set of 80 I-53 module *I–V* curves.

during the period of 20 minutes: the irradiance increased from 845 to around 900 W/m^2 and the temperature from 33 to 49 °C.

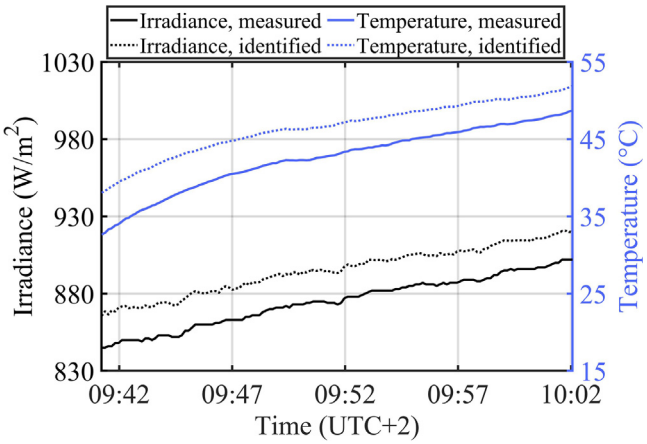

Fig. 7. Measured and identified irradiance and temperature for the set of 140 ISF-145 module *I–V* curves.

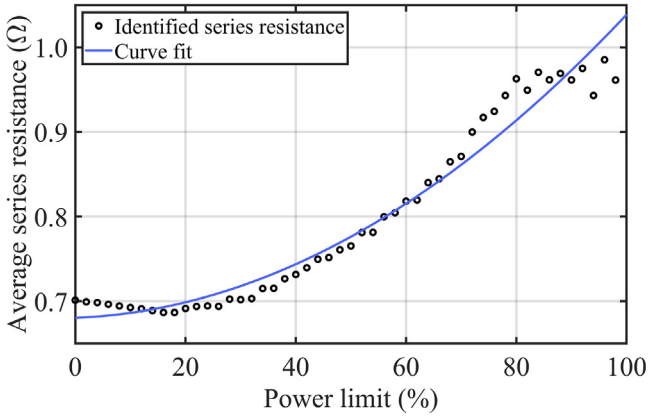

Fig. 8. Average identified series resistance for the 10 I-53 module *I–V* curves as a function of the power limit and the fitted curve of Eq. (8) to the values.

Table 4
Fitted constant values of the proposed polynomial function of Eq. (8) for the studied PV modules.

Fitting constant	ISOFOTON I-53	ISOFOTON ISF-145
c_1 (Ω)	0.3331	0.01766
c_2 (Ω)	0.02509	0.02448
c_3 (Ω)	0.6804	0.1895

3. Experimental validation

3.1. Fitting constants

Eq. (8) was fitted to the average series resistance as a function of PL of 10 measured *I–V* curves to obtain values for the constants c_1, c_2, and c_3 for both PV modules. The identified average series resistances and the curve fits are presented in Figs. 8 and 9 for the I-53 and ISF-145 modules, respectively. The fitted curves nicely represent the behavior of the average series resistance as a function of the PL, especially for the ISF-145 module. The values for fitting constants c_1, c_2, and c_3 are compiled in Table 4.

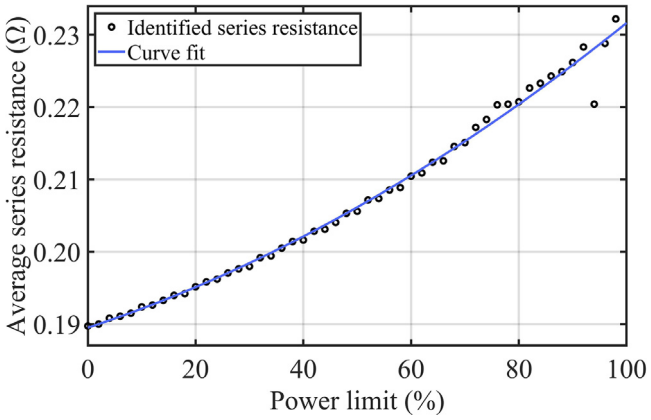

Fig. 9. Average identified series resistance for the 10 ISF-145 module *I–V* curves as a function of the power limit and the fitted curve of Eq. (8) to the values.

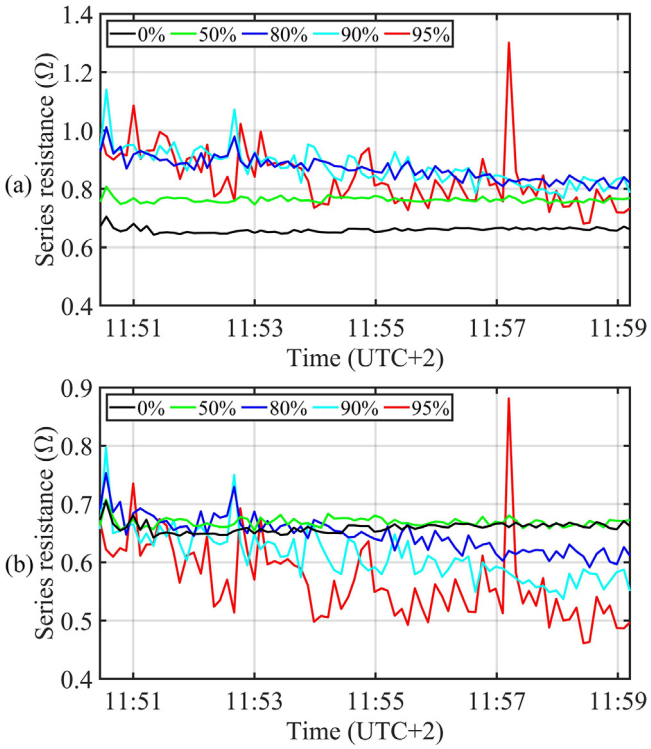

Fig. 10. Unscaled (a) and scaled (b) series resistances identified from the partial *I–V* curves with different power limits for the 80 *I–V* curves of the I-53 module. The black curve represents the series resistance identified using entire *I–V* curves. (For interpretation of the references to color in this figure legend, the reader is referred to the web version of this article.)

3.2. Estimated series resistances

The series resistance values obtained with partial *I–V* curves were scaled by Eq. (10) using the values obtained for constants c_1, c_2, and c_3 in Section 3.1 (Table 4). The unscaled and scaled series resistance values identified from partial curves cut using power limits of 50%, 80%, 90%, and 95% are presented in Fig. 10 for the 80 *I–V* curves of the I-53 module. As expected, the unscaled series resistances identified from the partial curves were higher than the values obtained from the whole curves. Moreover, variation in the identified unscaled values increased with

Table 5
Average relative differences (%) of the unscaled and scaled series resistance values identified from partial *I–V* curves from the values obtained from entire curves for the 80 measured I-53 module curves.

Power limit (%)	Unscaled	Scaled
50	15.74	1.45
60	20.13	0.25
70	24.69	−1.48
80	31.89	−1.78
90	32.62	−7.24
95	27.26	−13.83
98	23.84	−17.79

the increasing PL. The unscaled series resistance identified with the 50% PL was nearly constant, but about 15% higher than the one obtained from the whole curves. The scaled values were much closer to the values obtained from the whole curves than the unscaled ones. Especially, the scaled series resistance identified with the 50% PL almost overlaps with the curve representing the series resistance identified using the entire *I–V* curves. Moreover, the scaled values varied less than the unscaled values.

The average relative differences between the series resistances identified from the partial curves corresponding to different PL values and the values obtained from the entire curves are compiled in Table 5 for the 80 *I–V* curves of the I-53 module. As already observed in Fig. 10, the unscaled values clearly overestimated the series resistance with respect to the values identified using the entire *I–V* curves. The average difference in the unscaled series resistance was 16% with 50% PL and from 20% to 33% with higher PL values. The average differences in the scaled series resistances were much smaller than in the unscaled ones illustrating the functionality of the proposed method. The scaled series resistances obtained with 50% to 80% PL values were on the average within 2% of the values obtained with the whole curves. The average difference in the scaled series resistance increased with increasing PL, being 18% when using measurements within only 2% of the maximum power, but was much smaller than in the unscaled series resistance.

Fig. 11 shows the unscaled and scaled series resistance values identified from the partial *I–V* curves of the ISF-145 module. Again, the unscaled series resistances identified from the partial curves were higher than the values obtained from the whole curves and the difference as well as the variation of the identified values increased with increasing PL. The scaled series resistances obtained with all the PL values were close to, but slightly smaller than, the series resistances obtained from the whole curves.

The average relative differences between the series resistances identified from the partial *I–V* curves corresponding to different PL values and the values obtained from the entire curves are presented in Table 6 for the 140 *I–V* curves of the ISF-145 module. The average difference in the unscaled series resistance increased from 8% to 20% when the PL increased from 50% to 98%. The proposed series resistance determination method shows very high accuracy for this dataset. The scaled series resistances up to the PL of 98%, i.e., using only the points within 2% of the maximum power, were on the average within 2% of the series resistances obtained with the whole *I–V* curves.

4. Discussion

The proposed method is aimed assisting condition monitoring of PV modules from measurements performed near the MPP. The proposed method is useful in condition monitoring since increased series resistance indicates aging and faults of the modules [15]. The accuracy of the proposed method was illustrated by comparing the series resistance values obtained from partial *I–V* curves by the proposed method to the values identified from entire curves. The series resistance has been found to be dependent on the operating temperature [6,14] and irradiance [24]. In condition monitoring, the effects of operating conditions should be considered to distinguish them from the effects of aging and faults. However, PV module irradiance and temperature measurements are rarely available in practical PV sites. Thus, the proposed method should be used together with an identification procedure which identifies the series resistance jointly with the operating irradiance and temperature. In practical applications, it would be

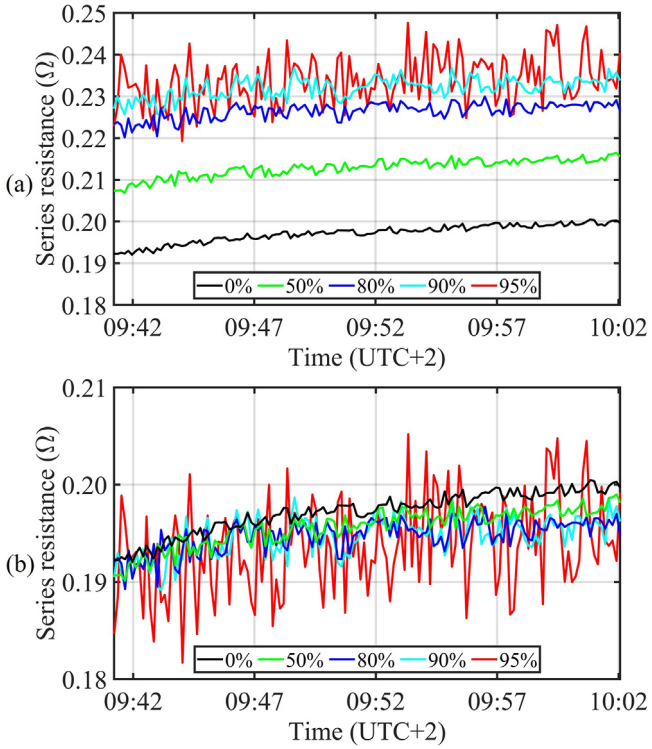

Fig. 11. Unscaled (a) and scaled (b) series resistances identified from the partial *I–V* curves with different power limits for the 140 *I–V* curves of the ISF-145 module. The black curve represents the series resistance identified using entire *I–V* curves. (For interpretation of the references to color in this figure legend, the reader is referred to the web version of this article.)

Table 6
Average relative differences (%) of the unscaled and scaled series resistance values identified from partial *I–V* curves from the values obtained from entire curves for the 140 measured ISF-145 module curves.

Power limit (%)	Unscaled	Scaled
50	7.96	−0.77
60	9.88	−1.11
70	11.94	−1.47
80	14.86	−1.23
90	17.68	−1.26
95	18.59	−1.74
98	20.22	−1.14

advisable to convert the obtained series resistance values to STC, utilizing the identified irradiance and temperature values, and to observe changes in the STC value of the series resistance.

Operating conditions during the measurement periods of 10 *I–V* curves, which were used to obtain the values for constants c_1, c_2, and c_3 in Section 3.1, were not stable. While the irradiances were almost constant (Fig. 4) the temperatures increased gradually (Fig. 5). The increase of temperature was a bit lower for the ISF-145 module than for the I-53 module. Moreover, the temperature during the measurement period of 10 *I–V* curves was much closer to the average temperature during the rest of the measurement period for the ISF-145 module (Fig. 7) than for the I-53 module (Fig. 6). As mentioned earlier, the operating temperature affects the series resistance. Thus, these temperature differences between the modules might be one reason why the accuracy of the proposed method was better for the ISF-145 module than for the I-53 module.

The irradiance and temperature values identified by the fitting procedure repeated the changes in the measured values very well for the ISF-145 module, i.e., the measured and identified curves in Figs. 4, 5 and 7 are of similar shape. For the I-53 module, the difference between the measured and identified values varied more between the *I–V* curves. The difference between the measured and identified temperature values varied clearly during the period of 10 *I–V* curves (black curves in Fig. 5) and during the rest of the measurement period (blue curves in Fig. 6). There was also some variation in the difference between the measured and identified irradiance values in Fig. 6. This indicates that the identification procedure of [17] works better for the ISF-145 module than for the I-53 module. Lower accuracy of the identification procedure in the case of the I-53 module could reduce the performance of the proposed method for that module. Moreover, the I-53 module was quite old and degraded compared to the ISF-145 module, which could also reduce the performance of the proposed method in the case of the I-53 module.

5. Conclusions

In this paper, a novel method to determine the series resistance of a PV module from *I–V* curves measured near the MPP has been proposed. The identified series resistance typically increases when the portion of the *I–V* curve that is used for the series resistance identification process becomes smaller and smaller around the MPP. The proposed method is based on the idea that the increase of the series resistance with the decreasing portion of the *I–V* curve considered is modeled mathematically, and the model is then used to scale the identified series resistance values obtained near the MPP to the values corresponding to the whole curve.

The proposed method has been experimentally validated using *I–V* curves of two PV modules measured in Malaga, Spain. First, a second-degree polynomial curve has been fitted to the average series resistance as a function of decreasing share of the *I–V* curve in the vicinity of the MPP of 10 measured *I–V* curves. After that, the series resistance values obtained with partial *I–V* curves have been scaled utilizing the obtained fitted polynomial function. To demonstrate the functionality and accuracy of the proposed method, the series resistance has been identified from partial *I–V* curves in the vicinity of the MPP having at least 50%, 60%, 70%, 80%, 90%, 95%, and 98% of the MPP power.

The results show that the series resistance can be accurately determined from measurements performed near the MPP. All the scaled series resistances for both PV modules and with all the considered power limits were much closer to the values of the whole curves than the unscaled ones. The results obtained with an ISOFOTON ISF-145 PV module are particularly promising: the scaled series resistances obtained up to the power limit of 98%, i.e., using only the measurements within 2% of the maximum power, were on the average within 2% of the series resistances obtained using the whole curves. Application of the proposed method at a PV string level is an interesting topic for continuing this study.

CRediT authorship contribution statement

Kari Lappalainen: Conceptualization, Methodology, Formal analysis, Writing – original draft. **Michel Piliougine:** Data Curation, Writing – review & editing. **Seppo Valkealahti:** Writing – review & editing. **Giovanni Spagnuolo:** Conceptualization, Writing – review & editing.

Acknowledgments

This work was supported by Business Finland, by the Academy of Finland (funding decision 348701) and by the Ministero dell'Istruzione, dell'Università e della Ricerca (Italy) under Grant PRIN2020–HOTSPHOT 2020LB9TBC. The authors acknowledge the University of Malaga for having made available the experimental datasets used in the paper.

References

[1] A. Abbassi, R. Ben Mehrez, B. Touaiti, L. Abualigah, E. Touti, Parameterization of photovoltaic solar cell double-diode model based on improved arithmetic optimization algorithm, Optik 253 (2022) 168600, http://dx.doi.org/10.1016/j.ijleo.2022.168600.

[2] M. Abdel-Basset, R. Mohamed, R.K. Chakrabortty, K. Sallam, M.J. Ryan, An efficient teaching-learning-based optimization algorithm for parameters identification of photovoltaic models: Analysis and validations, Energy Convers. Manage. 227 (2021) 113614, http://dx.doi.org/10.1016/j.enconman.2020.113614.

[3] F. Ali, A. Sarwar, F. Ilahi Bakhsh, S. Ahmad, A. Ali Shah, H. Ahmed, Parameter extraction of photovoltaic models using atomic orbital search algorithm on a decent basis for novel accurate RMSE calculation, Energy Convers. Manage. 277 (2023) 116613, http://dx.doi.org/10.1016/j.enconman.2022.116613.
[4] N. Anani, H. Ibrahim, Adjusting the single-diode model parameters of a photovoltaic module with irradiance and temperature, Energies 13 (12) (2020) 3226, http://dx.doi.org/10.3390/en13123226.
[5] E.I. Batzelis, S.A. Papathanassiou, A method for the analytical extraction of the single-diode PV model parameters, IEEE Trans. Sustain. Energy 7 (2016) 504–512, http://dx.doi.org/10.1109/TSTE.2015.2503435.
[6] D.T. Cotfas, P.A. Cotfas, O.M. Machidon, Study of temperature coefficients for parameters of photovoltaic cells, Int. J. Photoenergy 2018 (2018) 5945602, http://dx.doi.org/10.1155/2018/5945602.
[7] W. De Soto, S.A. Klein, W.A. Beckman, Improvement and validation of a model for photovoltaic array performance, Sol. Energy 80 (2006) 78–88, http://dx.doi.org/10.1016/j.solener.2005.06.010.
[8] N. Femia, G. Petrone, G. Spagnuolo, M. Vitelli, Power Electronics and Control Techniques for Maximum Energy Harvesting in Photovoltaic Systems, Taylor & Francis Group, Boca Raton, 2013.
[9] F.P. García Márquez, I.S. Ramírez, Condition monitoring system for solar power plants with radiometric and thermographic sensors embedded in unmanned aerial vehicles, Measurement 139 (2019) 152–162, http://dx.doi.org/10.1016/j.measurement.2019.02.045.
[10] M. Hejri, H. Mokhtari, On the comprehensive parametrization of the photovoltaic (PV) cells and modules, IEEE J. Photovolt. 7 (2017) 250–258, http://dx.doi.org/10.1109/JPHOTOV.2016.2617038.
[11] Á. Huerta Herraiz, A. Pliego Marugán, F.P. García Márquez, Photovoltaic plant condition monitoring using thermal images analysis by convolutional neural network-based structure, Renew. Energy 153 (2020) 334–348, http://dx.doi.org/10.1016/j.renene.2020.01.148.
[12] H. Kalliojärvi, K. Lappalainen, S. Valkealahti, Feasibility of photovoltaic module single-diode model fitting to the current–voltage curves measured in the vicinity of the maximum power point for online condition monitoring purposes, Energies 15 (2022) 9079, http://dx.doi.org/10.3390/en15239079.
[13] H. Kalliojärvi-Viljakainen, K. Lappalainen, S. Valkealahti, A novel procedure for identifying the parameters of the single-diode model and the operating conditions of a photovoltaic module from measured current–voltage curves, Energy Rep. 8 (2022) 4633–4640, http://dx.doi.org/10.1016/j.egyr.2022.03.141.
[14] F. Khan, S.-H. Baek, J.H. Kim, Wide range temperature dependence of analytical photovoltaic cell parameters for silicon solar cells under high illumination conditions, Appl. Energy 183 (2016) 715–724, http://dx.doi.org/10.1016/j.apenergy.2016.09.020.
[15] D.L. King, M.A. Quintana, J.A. Kratochvil, D.E. Ellibee, B.R. Hansen, Photovoltaic module performance and durability following long-term field exposure, Prog. Photovolt., Res. Appl. 8 (2000) 241–256.
[16] K. Lappalainen, P. Manganiello, M. Piliougine, G. Spagnuolo, S. Valkealahti, Virtual sensing of photovoltaic module operating parameters, IEEE J. Photovolt. 10 (2020) 852–862, http://dx.doi.org/10.1109/JPHOTOV.2020.2972688.
[17] K. Lappalainen, M. Piliougine, G. Spagnuolo, Experimental comparison between various fitting approaches based on RMSE minimization for photovoltaic module parametric identification, Energy Convers. Manage. 258 (2022) 115526, http://dx.doi.org/10.1016/j.enconman.2022.115526.
[18] A.K. Panchal, *I–V* data operated high-quality photovoltaic solution through per-unit single-diode model, IEEE J. Photovolt. 10 (2020) 1175–1184, http://dx.doi.org/10.1109/JPHOTOV.2020.2996711.
[19] G. Petrone, C.A. Ramos-Paja, G. Spagnuolo, Photovoltaic Sources Modeling, John Wiley & Sons, Chichester, 2017.
[20] J.C.H. Phang, D.S.H. Chan, J.R. Phillips, Accurate analytical method for the extraction of solar cell model parameters, Electron. Lett. 20 (1984) 406–408.
[21] M. Piliougine, J. Carretero, L. Mora-Lopez, M. Sidrach-de Cardona, Experimental system for current–voltage curve measurement of photovoltaic modules under outdoor conditions, Prog. Photovolt. Res. Appl. 19 (2011) 591–602, http://dx.doi.org/10.1002/pip.1073.
[22] M. Piliougine, R.A. Guejia-Burbano, G. Petrone, F.J. Sanchez-Pacheco, L. Mora-Lopez, M. Sidrach-de Cardona, Parameters extraction of single diode model for degraded photovoltaic modules, Renew. Energy 164 (2021) 674–686, http://dx.doi.org/10.1016/j.renene.2020.09.035.
[23] M. Piliougine, A. Oukaja, M. Sidrach-de Cardona, G. Spagnuolo, Temperature coefficients of degraded crystalline silicon photovoltaic modules at outdoor conditions, Prog. Photovolt. Res. Appl. 29 (2021) 558–570, http://dx.doi.org/10.1002/pip.3396.
[24] C.S. Ruschel, F. Perin Gasparin, A. Krenzinger, Experimental analysis of the single diode model parameters dependence on irradiance and temperature, Sol. Energy 217 (2021) 134–144, http://dx.doi.org/10.1016/j.solener.2021.01.067.
[25] R. Singh, M. Sharma, R. Rawat, C. Banerjee, An assessment of series resistance estimation techniques for different silicon based SPV modules, Renew. Sustain. Energy Rev. 98 (2018) 199–216, http://dx.doi.org/10.1016/j.rser.2018.09.020.
[26] S. Spataru, D. Sera, T. Kerekes, R. Teodorescu, Diagnostic method for photovoltaic systems based on light *I–V* measurements, Sol. Energy 119 (2015) 29–44, http://dx.doi.org/10.1016/j.solener.2015.06.020.
[27] F.J. Toledo, J.M. Blanes, V. Galiano, Two-step linear least-squares method for photovoltaic single-diode model parameters extraction, IEEE Trans. Ind. Electron. 65 (2018) 6301–6308, http://dx.doi.org/10.1109/TIE.2018.2793216.
[28] J.R. Wilcox, A.W. Haas, J.L. Gray, R.J. Schwartz, Estimating saturation current based on junction temperature and bandgap, AIP Conf. Proc. 1407 (2011) 30–33, http://dx.doi.org/10.1063/1.3658288.
[29] S. Yadir, R. Bendaoud, A. EL-Abidi, H. Amiry, M. Benhmida, S. Bounouar, B. Zohal, H. Bousseta, A. Zrhaiba, A. Elhassnaoui, Evolution of the physical parameters of photovoltaic generators as a function of temperature and irradiance: New method of prediction based on the manufacturer's datasheet, Energy Convers. Manage. 203 (2020) 112141, http://dx.doi.org/10.1016/j.enconman.2019.112141.
[30] S. Yu, A.A. Heidari, G. Liang, C. Chen, H. Chen, Q. Shao, Solar photovoltaic model parameter estimation based on orthogonally-adapted gradient-based optimization, Optik 252 (2022) 168513, http://dx.doi.org/10.1016/j.ijleo.2021.168513.